Chemistry & Biology, Vol. 11, 1339–1350, October, 2004, ©2004 Elsevier Ltd. All rights reserved. DOI 10.1016/j.chembiol.2004.07.008

Molecular Dynamics Simulation Links Conformation of a Pore-Flanking Region to Hyperekplexia-Related Dysfunction of the Inhibitory Glycine Receptor

Hans-Georg Breitinger,[1] Harald Lanig,[2] Christine Vohwinkel,[1] Christof Grewer,[3,4] Ulrike Breitinger,[1] Tim Clark,[2] and Cord-Michael Becker[1,*]
[1]Institut für Biochemie
Emil-Fischer-Zentrum
[2]Computer-Chemie-Centrum
Friedrich-Alexander-Universität
Erlangen-Nürnberg
Erlangen
Germany
[3]Max-Planck-Institut für Biophysik
Frankfurt
Germany

Summary

Inhibitory glycine receptors mediate rapid synaptic inhibition in mammalian spinal cord and brainstem. The previously identified hyperekplexia mutation *GLRA1(P250T)*, located within the intracellular TM1-2 loop of the GlyR α1 subunit, results in altered receptor activation and desensitization. Here, elementary steps of ion channel function of α1(250) mutants were resolved and shown to correlate with hydropathy and molar volume of residue α1(250). Single-channel recordings and rapid activation kinetic studies using laser pulse photolysis showed reduced conductance but similar open probability of α1(P250T) mutant channels. Molecular dynamics simulation of a helix-turn-helix motif representing the intracellular TM1-2 domain revealed alterations in backbone conformation, indicating an increased flexibility in these mutants that paralleled changes in elementary steps of channel function. Thus, the architecture of the TM1-2 loop is a critical determinant of ion channel conductance and receptor desensitization.

Introduction

The strychnine-sensitive glycine receptor (GlyR), a member of the ligand-gated ion channel family, is the principal mediator of fast inhibitory synaptic transmission in the human brainstem and spinal cord [1–4]. Presently, four glycine binding α subunits (α1–4) and one structural β subunit of vertebrate GlyRs have been identified [5].

Despite considerable advances in the understanding of receptor function, comparatively little is known about the structure of ligand-gated ion channels. According to the classical topology model for acetylcholine receptor-type ion channels, five identical or homologous subunits assemble into a pentameric membrane complex [3]. For each subunit, the extracellular N-terminal domain comprises about 50% of the protein sequence, followed by four hydrophobic membrane-spanning segments (TM1–TM4). TM2 of each subunit points to the center of the complex, forming the inner lining of the central ion pore [5]. A large TM3-4 loop is thought to mediate intracellular interactions; the short C terminus is extracellular. To date, the X-ray structure of a molluscan acetylcholine binding protein (AChBP) represents the best model structure for the extracellular N-terminal domain of this ion channel superfamily [6]. This structure contains 8% of α helix, which is considerably less than found for the GlyR N-terminal domain by CD and FTIR spectroscopy (24%) [7]. Based on protease accessibility of reconstituted GlyRs, a different topology for parts of the N-terminal domain and TM1 was proposed, containing mainly β sheets in TM1 [8]. In contrast, a 4 Å electron microscopy structure of the nicotinic acetylcholine receptor from *Torpedo californica* [9] revealed considerable amounts of α helix in the protein. This structure shows that TM1 and TM2 are both α helical, connected by a short loop, thus forming a helix-turn-helix (HTH) motif, in agreement with the classical topology model of the GlyR. While secondary structure assignments of the N-terminal domain are diverse [7], the helical structure of the pore-lining TM2 has been demonstrated by NMR analysis for acetylcholine receptors [10] and GlyRs [11].

Mutations in the *GLRA1* gene encoding the α1 subunit of the GlyR underlie the human neurological disorder, hyperekplexia (STHE, stiff baby syndrome, OMIM #138491) [12]. The mutant allele *GLRA1(P250T)*, associated with a dominant form of hyperekplexia [13], encodes an amino acid exchange within the short intracellular TM1-2 loop. Proline 250 is highly conserved among ligand binding (α) subunits of the glycine/$GABA_{A/C}$ receptor anion channel family, but absent from the corresponding position of cation channels, such as nicotinic acetylcholine or 5-HT_3 receptors. The TM1-2 loop region has been recognized as part of the ion channel selectivity filter of acetylcholine-type ion channels [14]. Recombinant GlyR α1(P250T) channels disclosed reduced apparent agonist affinity as well as complete and rapid receptor desensitization. While individual channels could not be resolved, noise analysis suggested a reduced single-channel conductance [13]. Receptor desensitization and apparent ligand affinity were shown to be governed by the opposing action of hydrophobic volume versus charge in position α1(250) [15].

Here, analysis of elementary steps of GlyR channel function showed that the intracellular mutation α1(P250T) reduced channel conductance and stabilized the desensitized state, but had little effect on channel gating. Deletion of P250 resulted in a shift in EC_{50} but no dramatic changes in desensitization or conductance. Molecular dynamics (MD) simulations of the protein domain ranging from TM1 to TM2, using a simple helix-turn-helix motif based on published coordinates of this region, gave trends of backbone conformation and protein flexibility for the investigated α1(P250) mutants that correlated with ion channel desensitization and EC_{50} for glycine. Thus, MD simulation of a simple model system

*Correspondence: cmb@biochem.uni-erlangen.de
[4]Present address: Department of Physiology and Biophysics (R430), University of Miami School of Medicine, 1600 NW 10th Avenue, Miami, Florida 33136.

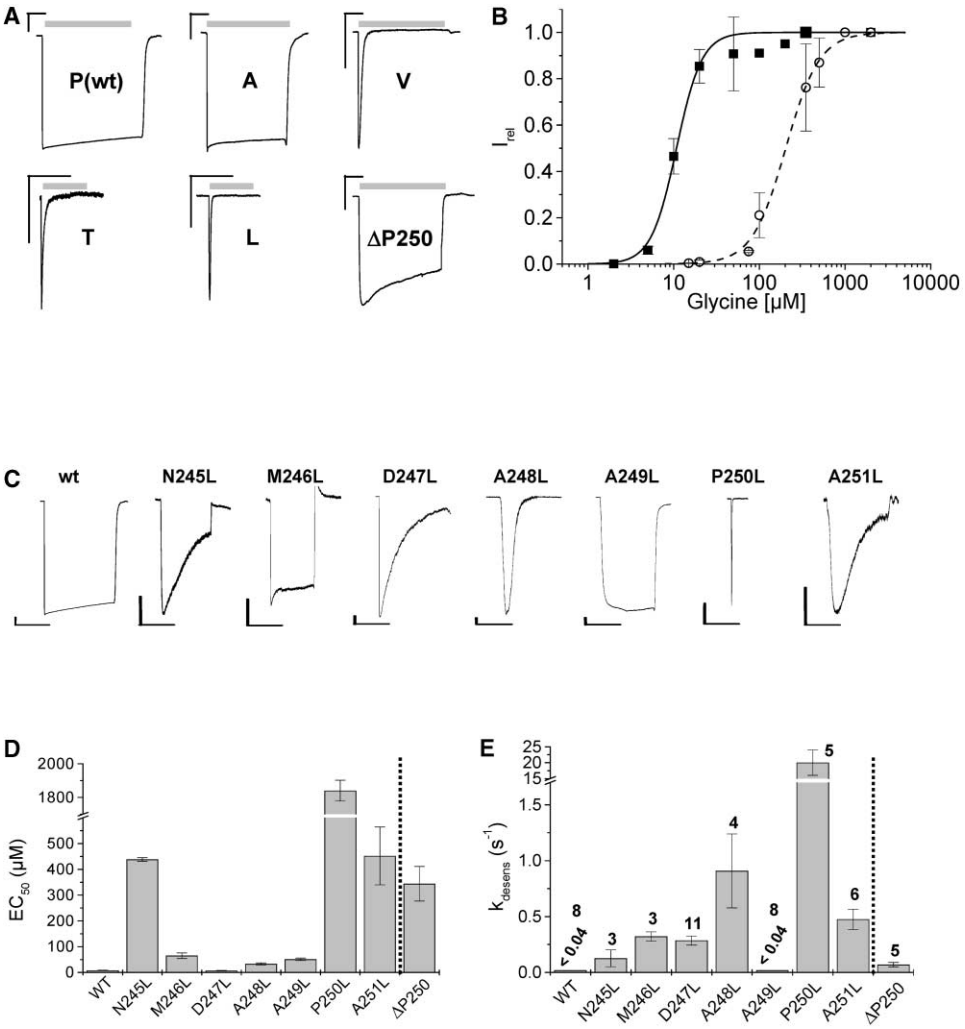

Figure 1. GlyR α1 Wild-Type and Mutant Whole-Cell Current Responses

(A) Whole-cell current responses to saturating concentrations of glycine. Residue 250 is indicated by the one-letter code. Vertical and horizontal scale bars are 500 pA and 2 s, respectively. Gray bars indicate glycine application. The observed time constants for desensitization of the wild-type and the mutant P250A were >20 s (2 mM glycine). Desensitization time constants were P250T: 0.11 s (10 mM glycine); P250V: 0.23 s (5 mM glycine); P250L: 0.036 s (10 mM glycine); ΔP250: 0.8 s (10% of current), >20 s (2 mM glycine). Except for the ΔP250 construct, desensitization of these mutants has been analyzed previously [15].

(B) Dose-response properties of α1(wt) and α1(ΔP250) current responses. Traces were fitted using the Hill equation. Constants were EC_{50} = 11 $\pm$ 1 μM, and n_{Hill} = 2.9 $\pm$ 0.5 for the wild-type (solid squares, solid line), and EC_{50} = 203 $\pm$ 9 μM, and n_{Hill} = 2.2 $\pm$ 0.1 for α1(ΔP250) (open circles, dashed line).

(C) Leucine-scan of the GlyR TM1-2 loop. Desensitization traces at saturating concentrations of 2 mM glycine are shown (10 mM for α1[P250L]). Horizontal and vertical scale bars are 5 s and 200 pA, respectively. Same traces for wild-type and P250L as in (A).

(D) EC_{50} values for whole-cell current responses of leucine mutants. Axis break is between 600 and 1700 μM. GlyR α1(ΔP250) data are shown for comparison.

(E) Desensitization rate constants for leucine mutants and the ΔP250 construct, obtained at saturating ligand concentration. Axis break is between 1.7 and 15 s^{-1}.

representing an excised receptor domain allowed the prediction of functional characteristics of the corresponding ion channel.

Results

Whole-Cell Current-Recording—Dose-Response Properties and Desensitization

Homomeric GlyR α1(wt) and α1(P250) mutant channels were expressed in HEK 293 cells, and glycine-mediated whole-cell currents recorded using rapid perfusion. Consistent with previous observations [13, 15], desensitization of whole-cell currents for wild-type and mutant receptors differed markedly. While wild-type and α1(P250A) currents desensitized to negligible extents (<5%, $\tau_{desens,sat.}$ > 25 s; Figure 1A), desensitization was dramatically increased for the mutants bearing large, hydrophobic side chains as well as for the hyperekplexia mutant α1(P250T) (desensitization 100%, $\tau_{desens,sat.}$ ~0.1 s; Figure 1A). Removal of the residue α1(P250) had no

Table 1. Receptor Characteristics of GlyR α1(245–251) Mutants (Means ± SD)

GlyR Variant	EC_{50} (μM)	k_{desens} (s^{-1})	Fraction I_{desens} (% I_{total})	n Cells
α1 wildtype	11 ± 1	<0.04	<5	8
α1(N245L)	438 ± 7	0.13 ± 0.08	75 ± 32	3
α1(M246L)	65 ± 11	0.32 ± 0.04	29 ± 7	3
α1(D247L)	7 ± 1	0.29 ± 0.04	82 ± 24	11
α1(A248L)	33 ± 4	0.91 ± 0.33	72 ± 39	4
α1(A249L)	51 ± 5	<0.04	<5	8
α1(P250L)	1840 ± 62	20 ± 4	100	5
α1(A251L)	452 ± 112	0.48 ± 0.09	90 ± 2	6
α1(ΔP250)	344 ± 116	0.07 ± 0.04 (1.96 ± 1.11)[a]	27 ± 25	3[a]

[a] Fast phase observed in 2 of 5 cells; 3 of 5 cells were used for EC_{50} determination.

significant effect on receptor desensitization (I_{desens} 27%, $\tau_{desens,sat.} > 15$ s; Figure 1A; Table 1).

Dose-response data yielded an ~19-fold difference in EC_{50}-values (wild-type: 11 ± 1 μM; α1(P250T): 192 ± 14 μM [15]). Hill coefficients n_{Hill} were 2.9 ± 0.5 for the wild-type and 2.2 ± 0.2 for the mutant [15] (Table 2). For the α1(ΔP250) receptors, a right-shift in dose-response curve was observed, the fitted constants were EC_{50} = 203 ± 9 μM, and n_{Hill} = 2.2 ± 0.1 (Figure 1B). The concentration dependence of maximum whole-cell currents (Figure 1B) was compatible with a 2-ligand model of receptor activation. We found neither improvement of fit nor significant alterations in the constants when a third ligand was included. This is reminiscent of a GlyR isoform expressed in embryonic mouse spinal neurons [16], and homomeric serotonin 5-HT_3 receptors [17]. Dose-response data comprise information from two equilibria, ligand binding and gating. Here, we used an independent technique—laser pulse photolysis (lpp)—to evaluate the gating constant ϕ. Resensitization, defined as the period between consecutive saturating glycine applications after which a maximum whole-cell current response could again be elicited from GlyR transfected HEK cells, was practically spontaneous for the wild-type ($\tau_{resens} < 5$ s, within the time resolution of the application system), but markedly slower for α1(P250T) mutant channels (τ_{resens} = 44 ± 3 s, not shown). Note that due to their large nondesensitizing current, wild-type receptors may not have desensitized completely during 10 s applications of glycine ($I_{steady\text{-}state} > 95\%$ of I_{max}), while all of the P250T channels were fully desensitized ($I_{steady\text{-}state}$ = 0) after ~2 s. Prolonged application of glycine (up to 60 s) to wild-type receptors confirmed the low extent and slow time course of desensitization. Strychnine inhibition of α1(P250T) currents was consistent with a competitive, or partially competitive inhibition mechanism [2] and indicated similar strychnine affinities for wild-type and P250T mutant receptors (not shown).

Table 2. Constants Describing Activation and Gating of Recombinant Homomeric Glycine Receptors (Means ± SD)

	α1(wt)	α1(P250T)
EC_{50} [μM]	11 ± 1[a]	192 ± 14[a,b]
n_{Hill}	2.9 ± 0.5[a]	2.2 ± 0.2[a,b]
I_{max} [pA]	4570 ± 100	2340 ± 50
τ_{resens} [s]	<5	44 ± 3
γ [pS]	69[d]	7[d] − 10[c]
k_{op} [s^{-1}]	1630 ± 40[e], 2200 ± 100[f]	818 ± 225[d]
k_{cl} [s^{-1}]	23 ± 2[e], 38 ± 30[f]	29 ± 9[d]
ϕ	0.014 ± 0.001[e], 0.017 ± 0.013[f]	0.035 ± 0.015[d]
P_{max}	0.99[e]	0.97[d]

[a] From dose-response curves.
[b] From [15].
[c] Cell-attached patch, slope conductance of main state.
[d] From outside-out patches.
[e] From laser-pulse photolysis.
[f] From [24].

Leucine Scan: Positional Effects within the GlyR TM1-2 Loop

To test whether the differences in EC_{50} values and desensitization rates of GlyR α1(P250) mutants were due to a specific position within the GlyR TM1-2 loop, a hydrophobic scan across this region was performed. Previously, we could show that leucine had the most pronounced effect on receptor desensitization and EC_{50} [15]. Thus, TM1-2 loop residues (i.e., N245–A251) were individually replaced by leucine. All mutants gave functional homomeric receptor channels, as assessed by whole-cell current recordings at saturating concentrations of glycine (Figure 1C; Table 1). Distinct patterns were observed for EC_{50} (Figure 1D) and receptor desensitization (Figure 1E). Distribution of EC_{50} values was reminiscent of a U-shaped positional dependence, with residues close to the putative membrane entry being most sensitive to hydrophobic substitution (Figure 1D), in marked contrast to the positional dependence of receptor desensitization rates (Figure 1E). Note that the mutant A249L, adjacent to position α1(250), was completely nondesensitizing, while both, EC_{50} and k_{desens} were highest for the P250L mutant. One possible explanation could be that two neighboring side chains in a polypeptide may not face in the same direction. It may, therefore, be assumed that desensitization is sensitive to the protein surface of the TM1-2 loop with the main determinant of desensitization being located at position α1(250).

Single-Channel Recordings—Conductance and Open State Dwell Time

Functional impairment of mutant receptor function may be due to (1) low protein expression, (2) reduced open probability, or (3) smaller single-channel conductance of mutant channels. To differentiate between these possibilities, we performed single-channel recording experi-

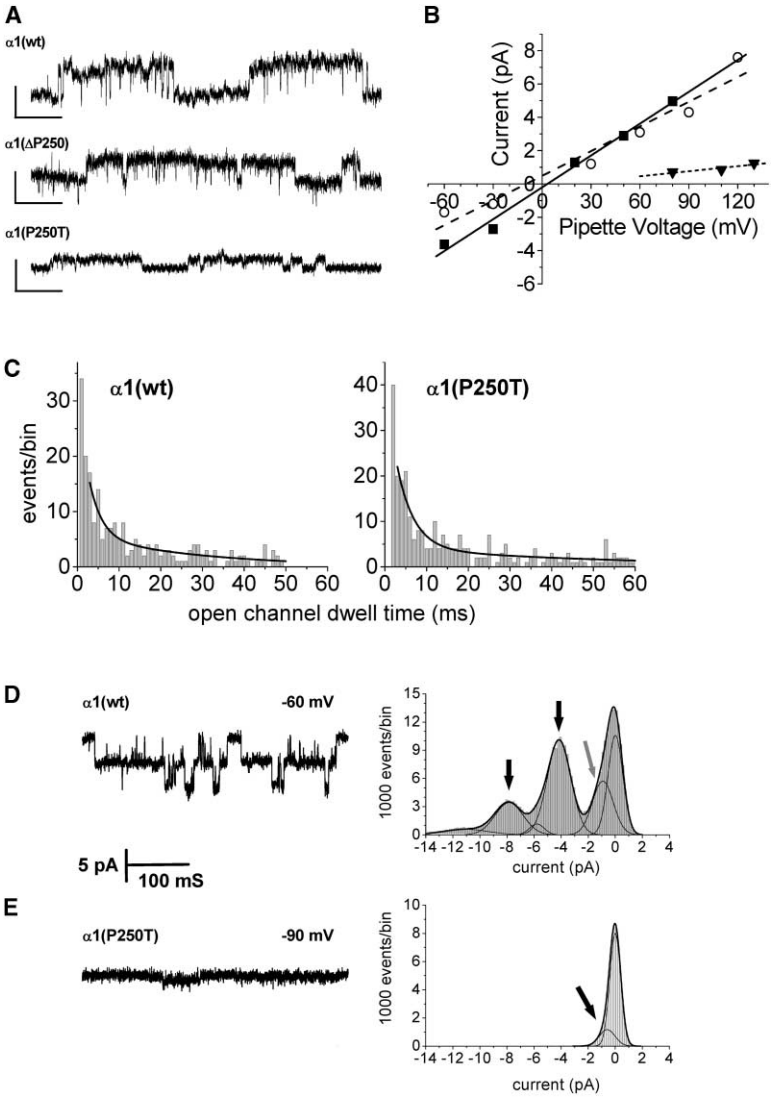

Figure 2. Single Channel Recordings

(A) Cell-attached single-channel recordings of α1(wt), α1(ΔP250), and α1(P250T) GlyRs. 1.5 s segments are shown; horizontal and vertical scale bars denote 5 pA and 200 ms, respectively. GlyR α1(wt): 5 μM glycine, $V_{pip} = +80$ mV; GlyR α1(ΔP250): 100 μM glycine, $V_{pip} = +60$ mV, GlyR α1(P250T): 20 μM glycine, $V_{pip} = +130$ mV.

(B) Current-voltage relationships using data from cell-attached recordings: GlyR α1(wt): $\gamma = 64 \pm 4$ pS (solid squares, solid line); GlyR α1(ΔP250): $\gamma = 49 \pm 6$ pS (open circles, broken line); GlyR α1(P250T): $\gamma = 10 \pm 4$ pS (solid triangles, dotted line). Note possible inward rectification for GlyR α1(ΔP250) currents; if only data points between −30 and +90 mV were used, the slope conductance was 47 ± 3 pS.

(C) GlyR α1(wt) and α1(P250T) open channel dwell times. The main conductance state observed in cell-attached recordings was analyzed; note that in the analyzed voltage range, GlyR gating kinetics are linear [19]. α1(wt): recordings at +80 mV and +50 mV were combined. Time constants for open state dwell times were 3.0 ± 1.3 ms (65%) and 28.8 ± 12.1 ms (35%). α1(P250T): recorded at +130 mV; open channel dwell time constants were 4.1 ± 0.9 ms (82%) and 54.0 ± 29.7 ms (18%).

(D) Outside-out single-channel recordings of α1(wt) receptors at −60 mV. Left: single-channel trace; right: all-point current histogram, baseline centered at 0 pA. Note multiple openings. Main transition: 4.15 pA at −60 mV (black arrow), corresponding to a main state conductance of 69 pS; a subconductance level of 15 pS is indicated (gray arrow).

(E) Outside-out single-channel recording of α1(P250T) channels at −90 mV, scale bars apply to traces in (D) and (E); one conductance level of 0.6 pA was detected (arrow), indicating a conductance of 7 pS.

ments. Cell-attached recordings from HEK 293 cells showed similar bursting behavior (Figure 2A) and slope conductance for wild-type and α1(ΔP250) constructs, indicating that chloride permeation across these channels was not significantly different (α1(wt): $\gamma_{slope} = 64 \pm 4$ pS, α1(ΔP250): $\gamma_{slope} = 49 \pm 6$ pS, Figure 2B). In contrast, α1(P250T) channels showed a dramatic reduction in unitary conductance, yet single channels could be resolved (Figure 2A). The transition corresponding to the level closest to baseline was fit with a linear regression yielding a slope conductance of ~10 pS (Figure 2B).

Wild-type single channels recorded from outside-out patches produced a main conductance level of ~69 pS (Figure 2D), in agreement with cell-attached recordings ($\gamma = 64$ pS, Figure 2B). This value was lower than the reported maximum conductance of 86 pS [18], but was reproducibly observed as the predominant conductance level with our line of HEK 293 cells. Under the same experimental conditions, α1(P250T) channels were hard to resolve in outside-out patches, resulting only in a slightly skewed current histogram (Figure 2E). The calculated conductance for α1(P250T) channels of 7 pS agreed with the value of 10 pS obtained from cell-attached recordings (Figure 2B).

Main state dwell-time histograms were constructed from cell-attached single-channel traces (Figure 2A), which had to be extensively filtered due to the low conductance of α1(P250T) mutant channels. The open-state dwell time histograms could be fit by double-exponential time courses (Figure 2C), yielding time constants for the wild-type of $\tau_{fast} = 3.0 \pm 1.3$ ms (65%), and $\tau_{slow} = 28.8 \pm 12.1$ ms (35%). For mutant channels, the time constants were $\tau_{fast} = 4.1 \pm 0.9$ ms (82%) and $\tau_{slow} = 54.0 \pm 29.7$ ms (18%), indicating that the mutation had no detectable effect on the open-close equilibrium of GlyR channels. Open state dwell time constants for the wild-type agreed with reported values [19]. Similar open channel dwell times for α1(wild-type) and α1(P250T) mutant channels were a necessary, but not sufficient, indication of unaltered gating in α1(P250T) receptors.

Laser-Pulse Photolysis-Direct Measurement of k_{op} and k_{cl}

As low conductances of mutant α1(P250T) receptors precluded a detailed single-channel analysis, channel gating was investigated by an additional, independent method. To this end, laser-pulse photolysis (LPP) was used as a rapid kinetic technique, allowing direct determination of the rate constants k_{op} and k_{cl} [20]. Upon irradiation with a 340 nm laser pulse, free glycine was released within less than 25 μs from its biologically inert precursor, α-CNB-caged glycine [19, 21]. LPP current traces for wild-type [19] and α1(P250T) mutant channels permitted an analysis of channel opening and closing rates (Figures 3A and 3B). Using the 2-ligand model of receptor activation, rate constants of $k_{cl} = 29 \pm 9\ s^{-1}$, and $k_{op} = 818 \pm 225\ s^{-1}$ were obtained from the intercept and the slope of the linear fit of the data according to equation 4 (Figure 3C). Constants for the wild-type were $k_{op} = 1630 \pm 40\ s^{-1}$ and $k_{cl} = 23 \pm 2\ s^{-1}$, in good agreement with previously reported values [19] (Table 2).

The LPP method does not require the release of saturating ligand concentrations, since the linear relationship given by equation 4 is valid over the entire concentration range [20]. The technique relies on the assumption that ligand binding occurs on a much faster time scale than channel-opening and closing, as previously shown for GlyRs, where the association rate for glycine of 10^7 $M^{-1}s^{-1}$ exceeds the channel-opening rate of 2200 s^{-1} by more than three orders of magnitude [19]. Nevertheless, ligand binding may become rate-limiting at low ligand concentrations. For the α1(P250T) mutant, k_{op} had to be extrapolated from measurements at low agonist concentration, since the technique has an upper limit of photorelease from caged glycine that was not saturating. While this might result in a higher error associated with numeric values of the rate constants, the principal results, namely that (1) k_{cl} is largely unchanged between wild-type and mutant receptors, and (2) $k_{op} >> k_{cl}$ for both GlyR constructs, are valid despite the limited agonist concentration range available for α1(P250T) channels.

Molecular Dynamics Simulation of the TM 1-2 Domain Structure

To identify alterations in the domain structure of the intracellular TM 1-2 loop that correlated with the observed changes in elementary steps of channel function, molecular dynamics (MD) simulations were carried out using a simple helix-turn-helix motif (Figure 4A). For TM2, coordinates from published NMR structures of model peptides of the nicotinic acetylcholine receptor [10] were used to generate the starting structures. This starting geometry was in good agreement with a recently published structure of the *Torpedo* nicotinic acetylcholine receptor at 4 Å resolution [9]. The entire motif, consisting of 64 residues, was placed in a simulated water box (Figure 4A) applying periodic boundary conditions; no explicit membrane fragment was included in the simulations. Energy minimization followed by MD equilibration and production was carried out for the wild-type and the mutants α1(P250A/S/T/V/L/F). In each case, wild-type coordinates served as identical geometrical basis. After modifying the mutant residue at position 250, the systems were geometry optimized and subjected to MD equilibration and production phases. The

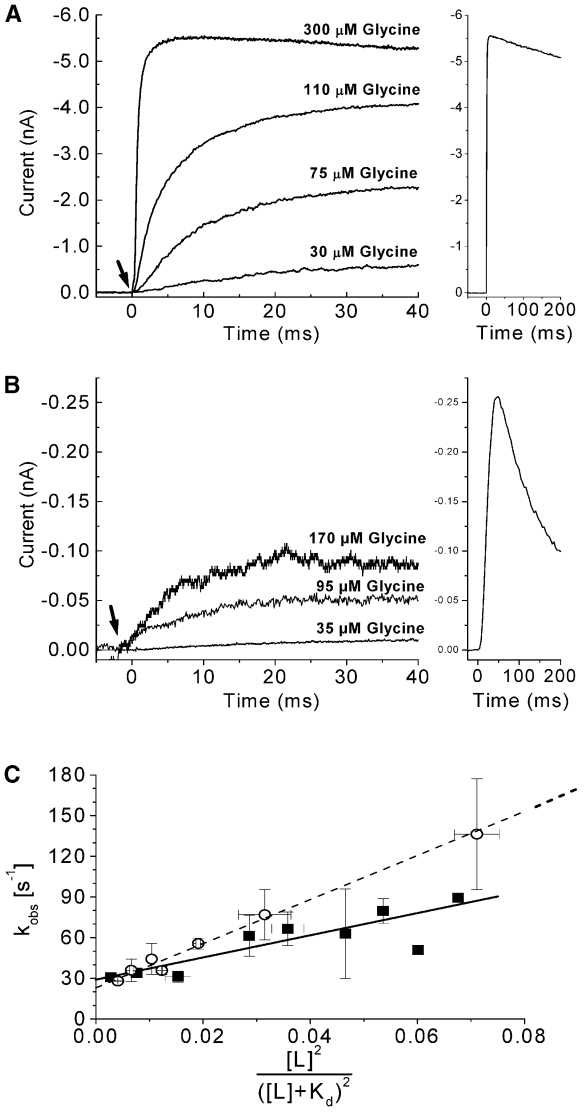

Figure 3. Laser-Pulse-Photolysis

Right hand panels show control flow experiments with 1 mM (wt) or 2 mM α1(P250T) glycine used for calibration. Left hand panels show scaled laser pulse photolysis traces. Typically, 2–8 mM caged glycine was flown over the cell and the laser fired at time 0 (arrow). I_{max} was determined and the concentration of liberated glycine determined by comparing to control flow measurements.

(A) GlyR α1(wt) control traces.

(B) Laser-pulse photolysis currents recorded from α1(P250T) receptors.

(C) Analysis of laser-pulse photolysis data (equation 5). Nineteen data points from eight individual cells were used for analysis. Data points corresponding to similar concentrations of liberated glycine were pooled; x-errors are indicated (and are smaller than the symbols in some cases). Using $K_d = 427$ μM (vd. Figure 1), time constants of $k_{op} = 818 \pm 225\ s^{-1}$ and $k_{cl} = 29 \pm 9\ s^{-1}$ were determined from the slope and the intercept, respectively of the linear regression. For the wild-type, 31 data points from 5 cells were used in the analysis; constants were $k_{op} = 1630 \pm 40\ s^{-1}$ and $k_{cl} = 23 \pm 2\ s^{-1}$.

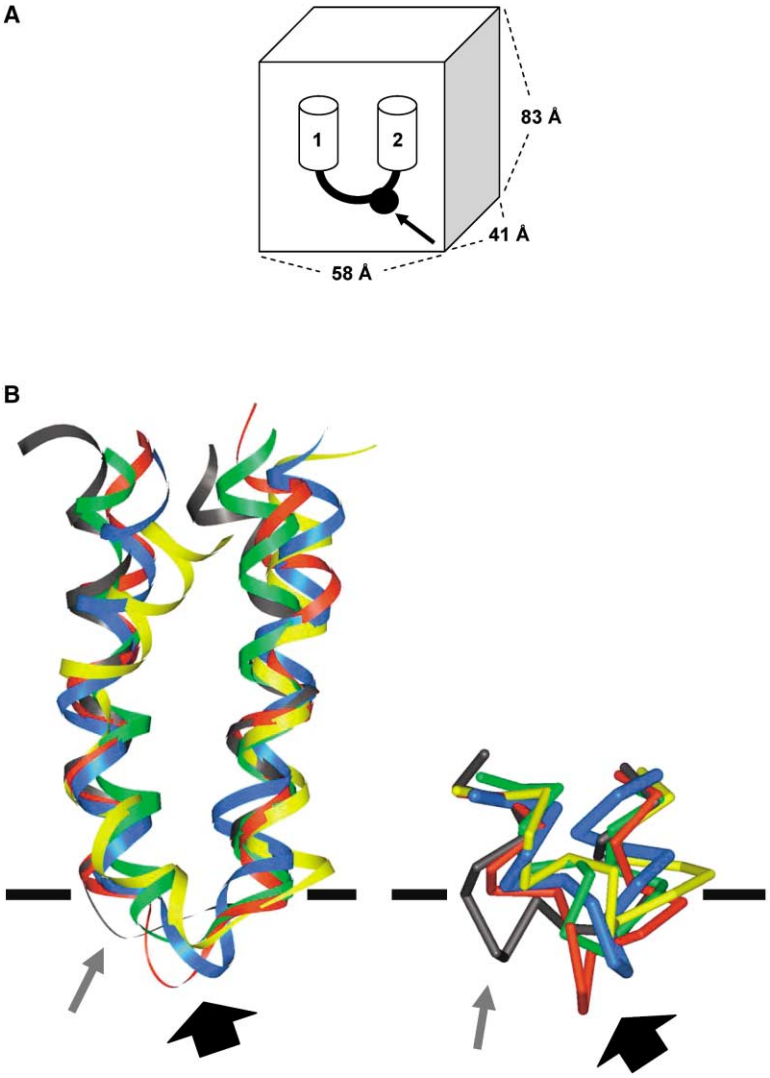

Figure 4. Molecular Dynamics Simulations of the TM 1-2 Loop of GlyR α1(P250) Mutants

(A) Schematic view of the helix-turn-helix system used for simulation.

(B) Peptide backbone of the calculated average structures of the GlyR α1(P250) wild-type (green), and the mutants α1(P250A) (yellow), α1(P250T) (blue), α1(P250L) (red), and α1(ΔP250) (gray), visualized as C_α trace. Note outward movement of the TM 1-2 loop for the hydrophobic mutants α1(P250T,L) (black arrow), and altered conformation for the deletion mutant α1(ΔP250) (gray arrow).

introduced residue types were chosen to reflect increasing hydrophobic volume in the critical position 250 [15]. Serine was included to detect potential effects of the hydroxyl function during the simulation.

To analyze the influence of the point mutations on the geometries of the different helix-turn-helix-motifs, we calculated for every mutant the average structure over each of the 200 snapshots sampled during the production phases of each molecular dynamics run. Each mutant average structure for the wild-type and α1(P250A,L) was overlaid on the average wild-type geometry by a root mean square (RMS) fit of the C_α coordinates of the protein backbone residues L233–I244 and V253–T258. Fitting over all residues of the model system appeared inappropriate because the long helices were both kinked during all simulations. Interestingly, the areas denoted above, which are located adjacent to the loop, perfectly maintained their helical secondary structure during the simulation. In contrast, P250 mutants with increasing side chain hydrophobicity (P250A/S/T/V/L) showed a gradual outward movement of the peptide backbone within the TM1-2 loop, exposing the protein region around position 250 (Figure 4B, black arrow), consistent with an altered protein surface presented to the cell interior at the TM1-2 loop. The calculated RMS values (Figure 5A) indicated a threshold above which pronounced desensitization was observed in the GlyR mutants. Alanine and serine, both producing wild-type-like receptor responses [15], showed the smallest overall deviation (Figures 4B and 5A). MD simulation of the construct α1(ΔP250), which was characterized by no or little desensitizing whole-cell current responses, gave an equilibrium loop conformation that differed from the wild-type (Figure 4B, gray arrow), but did not present the outward bulge that was observed in the hydrophobic mutants. Apparently, desensitization of mutant receptors in whole-cell current recordings coincided with a particular conformation observed in the MD simulations of the loop model system (Figure 4B).

The simulation results (Figure 4B) suggested that the equilibrium protein conformation of the two parallel helices of the helix-turn-helix motif was only slightly affected by structural disturbances in position α1(P250), while most of the deviations were located within the

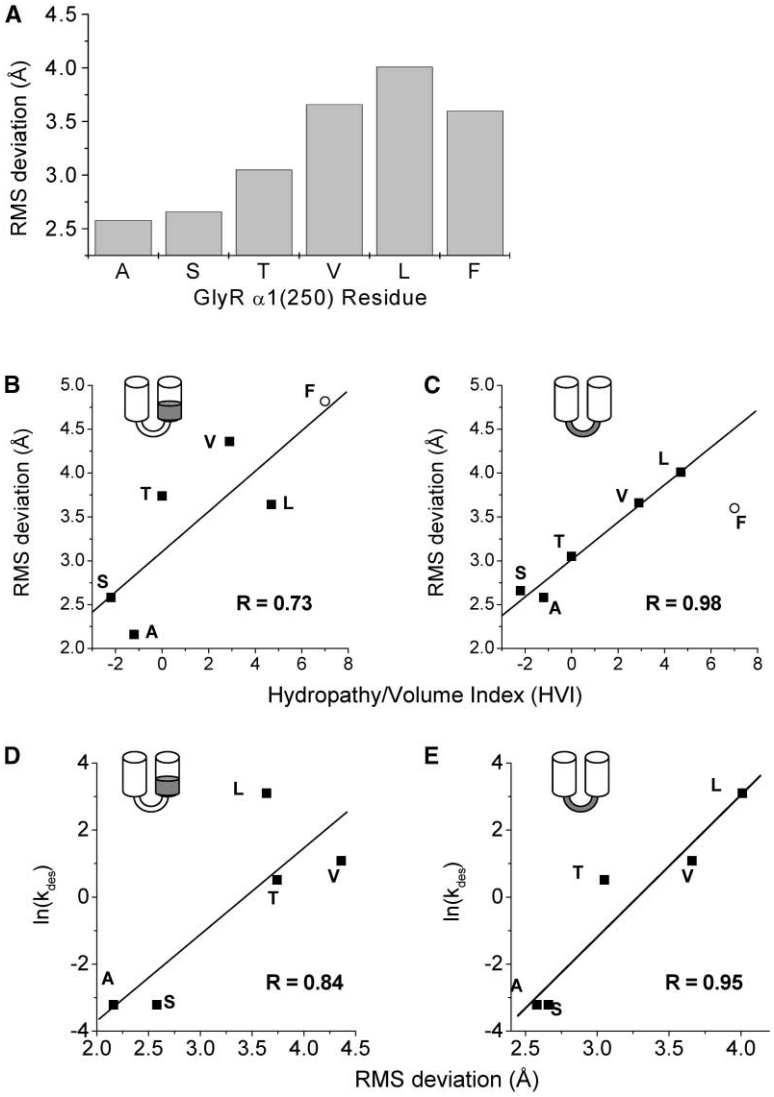

Figure 5. Molecular Dynamics Simulations of GlyR α1(P250) Mutants

Correlation between RMS deviations of the indicated protein region and the hydropathy/volume index (HVI) for residue 250. Increasing values of HVI indicate an increasing hydrophobic surface presented by the residue, RMS deviations served as a measure for local protein flexibility, R is the correlation coefficient.

(A) RMS deviation of the region covering the loop TM1-2 (residues N245–R252) calculated after fitting the mutant average structures (C_α atoms only) of the residues V235–I244, T258 to the wild-type.

(B) RMS deviation versus hydropathy/volume index (HVI) for the cytoplasmic half of TM 2.

(C) Correlation of RMS deviation versus HVI for the TM 1-2 loop. Note that in (B) and (C) the mutant P250F was not included in the fit, due to inconsistent electrophysiological properties of the construct GlyR α1(P250F) [15].

(D) Correlation of desensitization rates [$\ln(k_{des})$], of GlyR α1(P250) mutants versus RMS deviation for the cytoplasmic half of helix 2.

(E) Correlation of desensitization rates [$\ln(k_{des})$], of GlyR α1(P250) mutants versus RMS deviation for the TM 1-2 loop.

TM1-2 loop (Figures 4B and 5). To confine the influence of amino acid substitutions on the averaged geometries, we turned to an alternative description of the orientation of TM 2 in relation to TM 1. This could be achieved by fitting the C_α atoms of residues V235–I244, representing TM 1, and T258. The latter residue prevented the loop and TM 2 from rotation upon the helix axis of TM 1, which would potentially complicate interpretation of the simulation results. Based on this fit, Figure 5A shows the RMS C_α differences of residues N245 to T258, representing the TM1-2 loop and the N terminus of helix 2, respectively (note that the deletion mutant, α1[ΔP250], could not be used in these calculations, due to the different number of amino acid residues). RMS values of the α1(P250A/S) mutants showed only small geometric deviations from the wild-type. The hydrophobic residues α1(P250V/L/F) caused increasing RMS deviations from the wild-type coordinates in the protein region around and including the TM 1-2 loop (Figures 4B and 5B–5D). These RMS differences correlated closely with the hydropathy/volume index, HVI, for residue 250, which had previously been shown to be an empiric predictor for ion channel properties in GlyR α1(250) mutants [15]. RMS deviations of the entire motif could be broken down into separate contributions of TM 2 and the short loop. The correlation between HVI for residue 250 and the resulting RMS deviation of the TM 1-2 loop was excellent (Figure 5C, $R = 0.98$), being much stronger than for the cytoplasmic side of TM 2 (Figure 5B, $R = 0.73$). Note that the mutant α1(P250F) did not fit into this model, despite its increased hydrophobic volume. This is consistent with previous observations, where whole-cell current responses for the construct GlyR α1(P250F) were rarely observed, compared to >95% success rates for all other subunits [15]. Apparently, the effects of the phenylalanine side chain are not compatible with a regular GlyR function, and cannot be fully accounted for by MD simulations. The hyperekplexia mutant α1(P250T) was characterized by increased RMS deviation of the TM 1-2 loop region, similar to that of the hydrophobic mutants (Figures 4B and 5). Presence or absence of hydroxyl groups had no significant effect on simulation results or channel function, as evident from the comparison of the alanine and serine mutants, indicating that

specific hydrogen bonds or interactions with OH groups were not relevant. Rather, volume and hydrophobicity of residue α1(250), as reflected in the HVI, were the only determinants of backbone conformation. Given the ns time scale of the simulation, RMS deviation was taken as a measure for protein flexibility on the ms-s time scale of receptor desensitization. Indeed, correlation of $\ln(k_{des})$ of mutant receptor constructs versus RMS (Figures 5C and 5D) showed excellent correlation for the TM 1-2 loop (Figure 5E, $R = 0.95$), while correlation for the cytoplasmic face of helix 2 was considerably weaker (Figure 5D, $R = 0.84$). This indicated that desensitization was most sensitive to changes of protein flexibility in the TM 1-2 loop.

Discussion

The identification of protein domains that control ligand-gated ion permeation is a prerequisite to understand neurotransmitter receptor function and molecular pathology. Here, we investigated the intracellular hyperekplexia mutation α1(P250T) and related amino acid substitutions [13, 15] as a model for the dependence of elementary steps of GlyR activation and desensitization on subtle alterations of protein structure. Deviation of the TM1-2 loop from wild-type architecture was identified as an essential parameter of ion channel dysfunction. The functional impact could be correlated to structural changes observed by MD simulations of the excised protein motif.

In electrophysiological recordings, the apparent glycine affinity of α1(P250T) receptors was reduced by approximately one order of magnitude as compared to the wild-type. This is contrasted by radioligand binding studies [13, 15] and strychnine inhibition of glycine-induced whole-cell currents where both K_i for strychnine and equilibrium K_D for glycine were found to be unaffected by the mutation [15]. Discrepancies between equilibrium binding data and whole-cell current recordings suggest an involvement of elementary steps downstream of ligand binding, which are not accessible by equilibrium radioligand studies [22, 23]. Desensitization studies were consistent with the presence of distinct receptor states: wild-type receptors desensitized slowly, but resensitized rapidly, while the α1(P250T) mutant desensitized quickly and resensitized slowly. For the wild-type, desensitized and nondesensitized states appear to interconvert easily, suggesting similar thermodynamic stability. For α1(P250T) channels, rapid desensitization and slow current recovery indicated that the desensitized state was thermodynamically favored as compared to the wild-type, and both states would not interconvert in the continued presence of glycine. In addition to a lower conductance, the major functional consequence of the mutation α1(P250T) appeared to be a reduced ligand affinity of the nondesensitized receptor and a greatly increased stability of the inactivated state.

Analysis on the single-channel level indicated that the mutation α1(P250T) predominantly affected channel conductance, while the microscopic gating equilibrium, i.e., the transition between open and closed channel states, was essentially unchanged. This result was consistently obtained by three independent techniques: (1) concentration-dependence of wild-type and mutant whole-cell currents gave similar estimates for the gating constant ϕ, yielding an open probability near 1 for both constructs; (2) open-channel dwell times did not differ significantly between wild-type and mutant receptors; and (3) Laser-pulse photolysis using caged glycine [20] permitted a direct measurement of k_{op} and k_{cl}, which were not significantly different for α1 wild-type and α1(P250T) mutant receptors, indicating an almost identical P_{open} (Table 2). This is in contrast to the hyperekplexia mutation α1(K276E), located in the extracellular TM2-3 loop, where the principal effect of the mutation is on gating, as evident from unchanged main state conductance and reduced open channel dwell times [24].

A hydrophobic scan of the intracellular region GlyR α1(245–251) yielded two key results: (1) receptor activation and desensitization were independent processes, which showed different sensitivity toward modification of individual residues within the TM1-2 loop; and (2) GlyR α1(250) is by far the most critical position with respect to both receptor EC_{50} and desensitization. Recently, Wotring et al. showed that deletion of residue P(290)-corresponding to GlyR α1(P250)-in the ρ1 GABA receptor slightly reduced ion selectivity; the double mutation ρ1(ΔP290/A291E) resulted in a cation-selective GABA receptor [25]. It was concluded that alterations of effective charge near the cytoplasmic mouth of the channel pore affected ion selectivity [25]. Similar observations were reported for the GlyR α1(ΔP250) mutant, where removal of proline 250 resulted in slightly increased cation permeability [26], although these receptors were still found to be predominantly chloride selective. Our results for the α1(ΔP250) variant are in good agreement with reported data, indicating that excision of proline 250 predominantly affects pore size and selectivity rather than channel gating kinetics. Since the amino acid exchanges reported here left the effective charge of the TM1-2 loop unchanged (compare [25]), one should still expect all GlyR mutants studied here to be chloride channels. In a mutagenesis study of $GABA_A$ receptors, desensitization was shown to be sensitive to mutation of leucine 9¢ within TM 2 of α1β3γ2L receptors; introduction of hydroxylated residues resulted in prolonged channel openings, due to a decreased channel closing rate [27]. In this case, reduced hydrophobicity within TM 2 stabilized the open-channel state, thereby indirectly slowing macroscopic desensitization. Investigation of chimeric α1β3δ and α1β3γ2L $GABA_A$ receptors also implicated a region within TM2 in receptor desensitization [28]. Our experiments indicated that desensitization, but not the rates of channel opening and closing were affected by TM1-2 loop mutations. Thus, desensitization is probably not a homogenous process but is controlled by several domains of the receptor protein.

Structural effects of mutations in position α1(250) could be inferred by molecular dynamics simulations of the TM1-2 region assuming a helix-turn-helix motif. In a simple approach, coordinates for TM 2 from published NMR structures were used, and the motif was inserted into a water box. Energy minimization followed by extensive MD equilibration showed parallel trends for averaged backbone conformations and receptor current re-

sponses [15]. Rapidly desensitizing mutants showed an increasing deviation from the wild-type peptide backbone, primarily within the TM 1-2 loop. The deletion mutant α1(ΔP250) showed yet another backbone conformation, different from both the rapidly desensitizing mutants and the wild-type. This again paralleled channel properties of this mutant, which was non- or slowly desensitizing but had a reduced glycine affinity. Since the time scale of atom and molecule dynamics is much faster than the scale of protein interaction, the physiological consequence of GlyR α1(P250) mutations would be an increasingly hydrophobic protein surface at the TM 1-2 loop presented to the interior of the cell. Surprisingly, molecular modeling as well as functional analysis of the channel suggested that neither the particular conformation of proline, nor the presence of hydroxyl groups were of any consequence in this protein environment. Previously, analysis of electrophysiological data showed that an index HVI, reflecting only hydrophobicity and volume of an amino acid side chain actually predicted ion channel function of mutant GlyRs [15]. Here, MD simulation also found HVI to be the critical parameter determining TM 1-2 loop conformation.

Desensitization, i.e., the transition to the liganded, closed-channel state, might be envisaged as a refolding of the receptor protein. Since MD simulations were performed on a picosecond time scale, and receptor desensitization occurs on the order of milliseconds to seconds, RMS deviations should reflect local protein flexibility. Protein folding kinetics have been related to structural and orientational parameters of the polypeptide chain [29], observing logarithmic relationships [30]. Receptor desensitization at a saturating concentration of ligand will occur almost exclusively from the biliganded state (RL_2), and can thus be described by the single rate constant k_{des} [23]. Accordingly, we investigated how changes in k_{des} related to alterations of protein flexibility of the GlyR TM 1-2 loop, as expressed by the relation of RMS deviation $\sim \ln(k_{des})$. Indeed, RMS deviations in the TM 1-2 loop more closely correlated with changes in k_{des} than those of the cytoplasmic face of TM 2 (Figures 5C and 5D), indicating that protein flexibility at the short intracellular loop exerts a significant influence on receptor desensitization.

Conformation of the TM1-2 loop, and residue GlyR α1(P250) in particular, had a pronounced effect on GlyR function. It appears that the helix-turn-helix motif of the protein region around the TM1-2 loop forms an independent regulatory unit, as suggested by structural data [9] and the functional and modeling results presented here. The complementary approaches, kinetic analysis of wild-type and mutant GlyR function, and structure prediction on an atomic scale can thus be combined to give a more detailed understanding of structure-function relationships of ligand-gated ion channels.

Significance

The inhibitory GlyR (GlyR) is the predominant mediator of rapid synaptic inhibition in mammalian spinal cord and brainstem. GlyR defects underlie the human motor disorder, hyperekplexia (STHE, stiff baby syndrome), characterized by hypertonus, myoclonic seizures and increased startle reactions to external auditory or tactile stimuli. The GlyR belongs among the acetylcholine receptor-type superfamily of ligand-gated ion channels. In this family, a large body of data has been assembled from electrophysiological and biochemical investigation of receptor mutants, but detailed structural information is still scarce. Here, we present a study of elementary steps of GlyR activation and desensitization. A hyperekplexia mutation, GlyR α1(P250T), located within the short cytoplasmic loop preceding the actual ion channel region, as well as several α1(P250) mutants, including the deletion mutant α1(ΔP250) were generated and their ion channel properties investigated using patch-clamp recording techniques. Increased hydrophobic volume within the loop region resulted in rapidly desesensitizing, low-affinity receptor channels with position α1(250) being the most critical. Independently, molecular dynamics (MD) simulations of a helix-turn-helix motif representing the TM1-2 loop region of the receptor gave deviations in protein conformation consistent with increased backbone flexibility for mutant constructs, which showed an excellent correlation with functional characteristics obtained from patch-clamp studies. Thus, MD simulation of a simple model system allowed prediction of the corresponding GlyR ion channel properties. These results indicate that the short intracellular TM1-2 loop of the GlyR represents an independent regulatory domain whose structure-function relationship can now be unraveled.

Experimental Procedures

Site-Directed Mutagenesis

Single nucleotide exchanges corresponding to codons α1(245–251), as well as the P250 deletion were introduced by PCR-mediated site-directed mutagenesis as described [15]. All mutated clones were sequenced across the PCR-generated sequence to verify successful mutagenesis using the ABI sequencer system (ABI systems, Weiterstadt, Germany).

Whole-Cell Recording and Data Analysis

GlyR constructs were expressed in HEK 293 cells as described [15]. Whole-cell recording experiments were performed using an EPC9 amplifier controlled by Pulse software (HEKA electronics, Lambrecht, Germany). Recording pipettes (2–5 MΩ) were pulled from borosilicate glass (World Precision Instruments, Berlin, Germany) using a Sutter P-97 horizontal puller. Ligand application was carried out using a U-tube that bathed the suspended cell in a laminar flow and allowed ligand equilibration over the cell with a time resolution of 10–30 ms. The external buffer consisted of NaCl 137 mM, KCl 5.4 mM, $CaCl_2$ 1.8 mM, $MgCl_2$ 1.0 mM, and HEPES 5.0 mM (pH adjusted to 7.2 with NaOH); the internal buffer was CsCl 120 mM, $N(Et)_4Cl$ 20 mM, $CaCl_2$ 1.0 mM, $MgCl_2$ 2.0 mM, EGTA 11 mM, and HEPES 10 mM (pH adjusted to 7.2 with CsOH). Current responses were measured at room temperature, at a holding potential of -60 mV unless otherwise noted. Strychnine inhibition measurements were performed under conditions of simultaneous application of agonist and inhibitor. For laser-pulse photolysis experiments, the HEPES concentration was raised to 30 mM to counteract possible acidification of the solution upon dissolution of the caged compound.

Dose-response curves were constructed from the maximum current amplitudes and calculated by a nonlinear fitting routine using Microcal Origin (Additive, Friedrichsdorf, Germany). Dose-response data were normalized to the maximum response at saturating glycine concentration (2 mM). The Hill equation (equation 1) was used for analysis. As an additional check for consistency, data were ana-

lyzed according to a two-ligand model assuming independent binding sites [31].

$$I_{Gly} = \frac{I_{max}}{1 + \left(\frac{EC_{50}}{[Gly]}\right)^{nH}} \quad (1)$$

Here, I_{max} is the maximum observed current, I_{Gly} the current obtained at a given glycine concentration, EC_{50} the glycine concentration evoking half-maximum current amplitudes, and [*Gly*] the glycine concentration. For desensitization analysis of whole-cell current traces, the decaying current phase was analyzed (Microcal Origin) using a single or double exponential decay function plus a constant.

$$I_{obs} = I_1 * e^{-\frac{t}{\tau_1}} + I_2 * e^{-\frac{t}{\tau_2}} + I_{const.} \quad (2)$$

I_{obs} is the observed current, I_1 is the fraction of current amplitude decaying with time constant τ_1, I_2 is the fraction of current amplitude decaying with time constant τ_2, and $I_{const.}$ is the nondesensitizing current fraction. Generally, desensitization could be described satisfactorily using a single exponential function.

Single Channel Recording

For cell-attached recordings, pipettes of 5–10 MΩ resistance were filled with external buffer containing 5 μM glycine for α1(wt), 100 μM for α1(ΔP250), or 20 μM glycine for α1(P250T) constructs. For outside-out patches, pipettes were filled with intracellular buffer and the cell flow device was used for perfusion. Data were recorded at a sampling rate of 3–10 kHz, stored in ASCII format, converted to pCLamp format using Axoscope (Axon Instruments, Union City, CA), and analyzed using the programs Fetchan and Pstat from the pClamp 6 program suite (Axon Instruments). For all-point current histograms, data were used without further filtering. For open-channel dwell time histograms, data were refiltered at 1 kHz, and smoothed twice using a 7-point (wt), or 11-point (P250T) Savitzky-Golay algorithm prior to data conversion and analysis. Analysis was carried out by manually scanning the traces using pClamp 6 (Axon Instruments); doubtful events and multiple openings were discarded. Note that due to the low conductance of α1(P250T) channels, some noise remained after filtering, which was binned among the high-frequency transitions and may have increased the number of brief events in the dwell time histogram. The 2 ms component was, therefore, not considered in the analysis of open channel dwell times. Typical single-channel traces are given in Figure 2. The number of patches used for analysis were: α1(wt) cell-attached 5, outside-out 2; α1(P250T) cell-attached 7, outside-out 2; α1(ΔP250): cell-attached 2.

Laser-Pulse Photolysis

An EPC7 amplifier (HEKA) and pClamp 6 (Axon Instruments) software were used for data acquisition. After storage on a computer hard disk, individual current traces were analyzed offline using Microcal Origin software. αCNB-caged glycine [21], kindly provided by Professor G.P. Hess (Cornell University, Ithaca, NY), was flown over the cells at concentrations of 1 to 8 mM. Photoliberation was initiated by a 15 ns 340 nm laser pulse from a XeCl excimer laser-pumped dye laser using p-terphenyl (3 mM) in dioxan. Chloride currents were digitized at a rate of 10–50 kHz, and low-pass-filtered with a 3–10 kHz Bessel filter, prior to analysis. Calibration of the photo-released glycine concentration was carried out by using 1 mM or 2 mM glycine applied to the same cell by rapid perfusion and comparing Ipp- and flow current amplitudes. Values corresponding to similar concentrations of photoliberated glycine were pooled, errors for abscissa and ordinate are shown in Figure 3C (note that x-errors are smaller than the symbol size for some data points). Current rise reflects the transitions of the channel between open and closed states following a concentration jump of activating ligand and was fitted to [32]:

$$I(t) = I_{max} * (1 - e^{k_{obs}t}). \quad (4)$$

The individual time constants of channel opening and closing can be determined from the current rise time according to equation (5) [32]:

$$k_{obs} = k_{cl} + k_{op}\left[\frac{L}{L + K_d}\right]^2. \quad (5)$$

The channel gating equilibrium constant ϕ is then calculated as:

$$\phi = \frac{k_{cl}}{k_{op}}. \quad (6)$$

Calculation of the Combined Hydropathy/Volume Index, HVI

HVI was computed as described [15]. Briefly, the mean molar volume (vol(mean)) after [33]) of 14 proteinogenic amino acid residues (G,A,S,P,T,V,I, L,F,C,Y,R,Q,N) was calculated to be 88.8 ml/mol. The volume index for each residue was:

$$\frac{[\text{vol(residue)} - \text{vol(mean)}]}{10},$$

where values ranged from −4.5 to 3.5. These volume index values were added to the corresponding hydropathy indices after [34] without further weighting of the two indices. This procedure yielded a combined hydropathy/volume index, HVI, ranging from −10 (R) to 7 (F).

Three-Dimensional Structure of the Helix-Turn-Helix Motif

For the generation of the starting geometry of the wild-type P250, the amino acids F214 to V277 of the human GlyR α1 chain precursor sequence (SwissProt entry P23415, locus GRA1_HUMAN) were assumed to fold in a typical helix-turn-helix (HTH) motif (TM 1: 220–244; loop 1–2: 245–252; TM 2: 253–270). Alignment of the GRA1_HUMAN HTH fragment with the sequence of the TM 2 region of the *Torpedo californica* nicotinic acetylcholine receptor α subunit, for which the three-dimensional structure was solved by NMR spectroscopy (PDB entry 1DXZ), revealed sequence homology of the two TM 2 regions which justified the use of the nACh TM 2 coordinates for the generation of our HTH model. The TM 1 region of the HTH fragment was modeled as an ideal α helix. The backbone dihedral angles of the loop region were assumed in a way that both helix axes are almost parallel. To achieve optimal comparability of all simulations, this system always served as template for the generation of the point mutations at position P250, for which only the considered amino acid was replaced.

To validate our starting geometry for MD calculations, we extracted the TM1-loop-TM2 motif of the receptor α chain from coordinates (RCSB Database entry 1OED) of the *Torpedo* nicotinic acetylcholine receptor that had recently become available [9]. These coordinates were compared to our average mutant geometries by an RMS fit of the C_α coordinates of the model protein backbone residues L233–I244 and V253–T258 to the corresponding residues of the extracted receptor HTH-motif. Although within the starting geometry for our mutants, only TM2 was modeled according to experimental NMR data, the overall geometries of the MD averages were in excellent agreement with the structural data provided by electron-microscopic techniques. The RMSD values over the above residue range are smaller than 3 Å for all mutants. Considering the fact that the resolution of the receptor pore is only 4 Å, this comparison validates the geometry and assumptions of our model and justifies its use for the geometric and dynamic description of the TM1-2 loop motif under investigation.

Molecular Dynamics Simulations

All simulations were performed using the AMBER5 suite of programs and the previously established parm94 force field [35]. Each of the generated starting geometries was placed in a box of TIP3P water molecules, assuring that at least 10 Å were between the peptide and the edges of the box. To neutralize the overall system, two chloride ions were added according to the electrostatic potential of the peptide. The final system had a box size of 58 × 83 × 41 Å consisting of 64 amino acids, two chloride ions, and 4494 water molecules. For nonbonded interactions, a cutoff of 9 Å was used in all simulations with periodic boundary conditions. SHAKE was employed to keep all bonds involving hydrogen atoms rigid. The simulation time step was 1 fs with constant pressure conditions

(coupling constant 0.2 ps) and coupling the temperature to a heat bath with a time constant of 0.2 ps.

Prior to the molecular dynamics (MD) simulations, all systems were geometry optimized by 5000 cycles of conjugant gradient minimization to relax all atoms without any geometrical restraints. The general procedure for all MD simulations of the protein fragment in the water box comprises (1) heating the system to 300 K and equilibration for 400 ps and (2) production phase for 400 ps for data acquisition. During equilibration, the temperature was raised to 300 K and the solvent density stabilized around 1 g/cm^3. During the production phase, 200 snapshots of the actual geometries were collected as a trajectory for calculating average geometries with the AMBER module *carnal*, and for simulation stability control.

Acknowledgments

This work was supported by Deutsche Forschungsgemeinschaft (SFB 353), Bundesministerium für Bildung und Forschung, and the German-Israeli Foundation for Scientific Research and Development. We thank Professor George P. Hess for a gift of caged glycine, Professors Pjotr Bregestovski and Heinrich Sticht for helpful discussions, Drs. Kristina Becker and Carmen Villmann for a critical reading of the manuscript, and Rosa Weber for technical assistance.

Received: April 27, 2004
Revised: June 23, 2004
Accepted: July 14, 2004
Published: October 17, 2004

References

1. Betz, H., Kuhse, J., Schmieden, V., Laube, B., Kirsch, J., and Harvey, R.J. (1999). Structure and functions of inhibitory and excitatory glycine receptors. Ann. N Y Acad. Sci. *868*, 667–676.
2. Breitinger, H.G., and Becker, C.M. (1998). The inhibitory glycine receptor: prospects for a therapeutic orphan? Curr. Pharm. Des. *4*, 315–334.
3. Hucho, F., and Weise, C. (2001). Ligand-gated ion channels. Angew. Chem. Int. Ed. Engl. *40*, 3100–3116.
4. Unwin, N. (2002). Structure of the acetylcholine-gated channel. Novartis Found. Symp. *245*, 5–15.
5. Breitinger, H.G., and Becker, C.M. (2002). The inhibitory glycine receptor-simple views of a complicated channel. Chembiochem *3*, 1042–1052.
6. Brejc, K., van Dijk, W.J., Klaassen, R.V., Schuurmans, M., van Der Oost, J., Smit, A.B., and Sixma, T.K. (2001). Crystal structure of an ACh-binding protein reveals the ligand-binding domain of nicotinic receptors. Nature *411*, 269–276.
7. Breitinger, U., Breitinger, H.-G., Bauer, F., Fahmy, K., Glockenhammer, D., and Becker, C.-M. (2004). Conserved high affinity ligand binding and membrane association in the native and refolded extracellular domain of the human glycine receptor alpha1-subunit. J. Biol. Chem. *279*, 1627–1636.
8. Cascio, M. (2004). Structure and function of the glycine receptor and related nicotinicoid receptors. J. Biol. Chem. *279*, 19383–19386.
9. Miyazawa, A., Fujiyoshi, Y., and Unwin, N. (2003). Structure and gating mechanism of the acetylcholine receptor pore. Nature *424*, 949–955.
10. Opella, S.J., Marassi, F.M., Gesell, J.J., Valente, A.P., Kim, Y., Oblatt-Montal, M., and Montal, M. (1999). Structures of the M2 channel-lining segments from nicotinic acetylcholine and NMDA receptors by NMR spectroscopy. Nat. Struct. Biol. *6*, 374–379.
11. Yushmanov, V.E., Mandal, P.K., Liu, Z., Tang, P., and Xu, Y. (2003). NMR structure and backbone dynamics of the extended second transmembrane domain of the human neuronal glycine receptor alpha1 subunit. Biochemistry *42*, 3989–3995.
12. Becker, K., Becker, C.-M., and Breitinger, H.-G. (2000). The inhibitory glycine receptor as a model of hereditary channelopathies. In Channelopathies, F. Lehmann-Horn, ed. (Amsterdam: Elsevier).
13. Saul, B., Kuner, T., Sobetzko, D., Brune, W., Hanefeld, F., Meinck, H.M., and Becker, C.M. (1999). Novel GLRA1 missense mutation (P250T) in dominant hyperekplexia defines an intracellular determinant of glycine receptor channel gating. J. Neurosci. *19*, 869–877.
14. Corringer, P.J., Bertrand, S., Galzi, J.L., Devillers Thiery, A., Changeux, J.P., and Bertrand, D. (1999). Molecular basis of the charge selectivity of nicotinic acetylcholine receptor and related ligand-gated ion channels. Novartis Found. Symp. *225*, 215–224.
15. Breitinger, H.G., Villmann, C., Becker, K., and Becker, C.M. (2001). Opposing effects of molecular volume and charge at the hyperekplexia site alpha 1(P250) govern glycine receptor activation and desensitization. J. Biol. Chem. *276*, 29657–29663.
16. Walstrom, K.M., and Hess, G.P. (1994). Mechanism for the channel-opening reaction of strychnine-sensitive glycine receptors on cultured embryonic mouse spinal cord cells. Biochemistry *33*, 7718–7730.
17. Breitinger, H.-G., Geetha, N., and Hess, G.P. (2001). Inhibition of the 5–HT3 serotonin receptor by nicotine, cocaine and fluoxetine investigated by rapid chemical kinetic techniques. Biochemistry *40*, 8419–8429.
18. Bormann, J., Rundstrom, N., Betz, H., and Langosch, D. (1993). Residues within transmembrane segment M2 determine chloride conductance of glycine receptor homo- and hetero-oligomers. EMBO J. *12*, 3729–3737.
19. Grewer, C. (1999). Investigation of the α(1)-glycine receptor channel-opening kinetics in the submillisecond time domain. Biophys. J. *77*, 727–738.
20. Hess, G.P., and Grewer, C. (1998). Development and application of caged ligands for neurotransmitter receptors in transient kinetic and neuronal circuit mapping studies. Methods Enzymol. *291*, 443–473.
21. Grewer, C., Jager, J., Carpenter, B.K., and Hess, G.P. (2000). A new photolabile precursor of glycine with improved properties: a tool for chemical kinetic investigations of the glycine receptor. Biochemistry *39*, 2063–2070.
22. Colquhoun, D. (1998). Binding, gating, affinity and efficacy: the interpretation of structure-activity relationships for agonists and of the effects of mutating receptors. Br. J. Pharmacol. *125*, 924–947.
23. Breitinger, H.-G. (2001). Fast kinetic analysis of ligand-gated ion channels. Neuroscientist *7*, 95–103.
24. Lewis, T.M., Sivilotti, L.G., Colquhoun, D., Gardiner, R.M., Schoepfer, R., and Rees, M. (1998). Properties of human glycine receptors containing the hyperekplexia mutation α1(K276E), expressed in Xenopus oocytes. J. Physiol. *507*, 25–40.
25. Wotring, V.E., Miller, T.S., and Weiss, D.S. (2003). Mutations at the GABA receptor selectivity filter: a possible role for effective charges. J. Physiol. *548*, 527–540.
26. Lee, D.J., Keramidas, A., Moorhouse, A.J., Schofield, P.R., and Barry, P.H. (2003). The contribution of proline 250 (P-2′) to pore diameter and ion selectivity in the human glycine receptor channel. Neurosci. Lett. *351*, 196–200.
27. Bianchi, M.T., and Macdonald, R.L. (2001). Mutation of the 9′ leucine in the GABA(A) receptor γ2L subunit produces an apparent decrease in desensitization by stabilizing open states without altering desensitized states. Neuropharmacology *41*, 737–744.
28. Bianchi, M.T., and Macdonald, R.L. (2002). Slow phases of GABA(A) receptor desensitization: structural determinants and possible relevance for synaptic function. J. Physiol. *544*, 3–18.
29. Dill, K.A. (1999). Polymer principles and protein folding. Protein Sci. *8*, 1166–1180.
30. Makarov, D.E., and Plaxco, K.W. (2003). The topomer search model: a simple, quantitative theory of two-state protein folding kinetics. Protein Sci. *12*, 17–26.
31. Hess, G.P., Niu, L., and Wieboldt, R. (1995). Determination of the chemical mechanism of neurotransmitter receptor-mediated reactions by rapid chemical kinetic methods. Ann. N Y Acad. Sci. *757*, 23–39.
32. Matsubara, N., Billington, A.P., and Hess, G.P. (1992). How fast does an acetylcholine receptor channel open? Laser-pulse photolysis of an inactive precursor of carbamoylcholine in the microsecond time region with BC3H1 cells. Biochemistry *31*, 5507–5514.

33. Zamyatnin, A.A. (1972). Protein volume in solution. Prog. Biophys. Mol. Biol. *24*, 107–123.
34. Engelman, D.M., Steitz, T.A., and Goldman, A. (1986). Identifying nonpolar transbilayer helices in amino acid sequences of membrane proteins. Annu. Rev. Biophys. Biophys. Chem. *15*, 321–353.
35. Cornell, W.D., Cieplak, P., Bayly, C.I., Gould, I.R., Merz, J., Ferguson, D.M., Spellmeyer, D.C., Fox, T., Caldwell, J.W., and Kollman, P.A. (1995). A second generation force field for the simulation of proteins, nucleic acids, and organic molecules. J. Am. Chem. Soc. *117*, 5179–5197.